

# New bounds on heavy axions with an X-ray free electron laser

Jack W. D. Halliday,<sup>1,2</sup> Giacomo Marocco,<sup>3</sup> Konstantin A. Beyer,<sup>4</sup> Charles Heaton,<sup>1</sup> Motoaki Nakatsutsumi,<sup>5</sup> Thomas R. Preston,<sup>5</sup> Charles D. Arrowsmith,<sup>1</sup> Carsten Baecht,<sup>6</sup> Sebastian Goede,<sup>5</sup> Oliver Humphries,<sup>5</sup> Alejandro Laso Garcia,<sup>6</sup> Richard Plackett,<sup>1</sup> Pontus Svensson,<sup>1</sup> Georgios Vacalis,<sup>1</sup> Justin Wark,<sup>1</sup> Daniel Wood,<sup>1</sup> Ulf Zastra,<sup>5</sup> Robert Bingham,<sup>7,8</sup> Ian Shipsey,<sup>1</sup> Subir Sarkar,<sup>1</sup> and Gianluca Gregori<sup>1</sup>

<sup>1</sup>*Department of Physics, University of Oxford, Parks Road, OX1 3PU, UK*

<sup>2</sup>*Blackett Laboratory, Imperial College London, SW7 2AZ, UK*

<sup>3</sup>*Lawrence Berkeley National Laboratory, 1 Cyclotron Road, Berkeley, CA 94720-8153, USA*

<sup>4</sup>*Max-Planck-Institut für Kernphysik Saupfercheckweg 1, 69117, Heidelberg, Germany*

<sup>5</sup>*European XFEL, Holzkoppel 4, 22869 Schenefeld, Germany*

<sup>6</sup>*Helmholtz-Zentrum Dresden-Rossendorf, Bautzner Landstraße 400, 01328 Dresden, Germany*

<sup>7</sup>*STFC, Rutherford Appleton Laboratory, Didcot OX11 0QX, UK*

<sup>8</sup>*John Anderson Building, University of Strathclyde, G4 0NG, UK*

(Dated: May 14, 2024)

We present new exclusion bounds obtained at the European X-ray Free Electron Laser facility (EuXFEL) on axion-like particles (ALPs) in the mass range  $10^{-3}$  eV  $\lesssim m_a \lesssim 10^4$  eV, which is relatively unconstrained by laboratory searches. Our experiment exploits the Primakoff effect via which photons can, in the presence of a strong external electric field, decay into axions, which then convert back into photons after passing through an opaque wall. While similar searches have been performed previously at a 3<sup>rd</sup> generation synchrotron [1], our work demonstrates improved sensitivity, exploiting the higher brightness of X-rays at EuXFEL.

*Introduction.* The axion arises from the breaking of Peccei-Quinn (PQ) symmetry [2–4], which was proposed to explain the absence of  $CP$ -violation by the strong interactions described by quantum chromodynamics (QCD). Axion-like particles (ALPs) also arise in string theory [5]. In spite of being very light and having suppressed couplings, coherent oscillations of relic axions can naturally account for cold dark matter if  $m_a \sim 10^{-6}$ – $10^{-4}$  eV [6–8]. Most laboratory searches for axions converting to photons in a magnetic field [9] have therefore focussed on this ‘light axion window’ [10], targeting axion-photon couplings corresponding to the Galactic halo dark matter being made of axions. This coupling is related (inversely) to the scale of PQ symmetry breaking in extensions of the Standard Model that implement the PQ symmetry, e.g. the Kim-Shifman-Vainshtein-Zakharov (KSVZ) model [11, 12] or the Dine-Fischler-Srednicki-Zhitnitsky (DFSZ) model [12, 13]. It has been noted that when the PQ symmetry (in the DFSZ model) is broken after cosmological inflation, axions are also produced by the decay of domain walls [14], and the preferred mass for axions to make up dark matter then exceeds  $10^{-2}$  eV [15]. Such ‘heavy’ axions are associated with a low scale of Peccei-Quinn symmetry breaking, so are theoretically preferred as being less susceptible to the ‘axion quality problem’, namely the potential destabilising effects of quantum gravity on global symmetries [16–18].

Stringent bounds on such heavy axions (excluding astrophysical arguments derived from stellar cooling [19]) come from the CERN Axion Solar Telescope (CAST) [20]. This is a ‘helioscope’ which looks for conversion of axions from the Sun into X-ray photons as they pass through a strong magnetic field. For  $m_a \gtrsim 1$  eV, the axion-photon conversion probability in such a static magnetic field becomes highly suppressed. Instead, Bragg

conversion in the electric field of crystals is then more efficient and underground searches for dark matter and  $\beta\beta$ -decay then place strong bounds on the axion-photon coupling [21–28]. However when the damping of X-rays in a crystal is taken into account, such bounds are considerably weakened [29]. Moreover, since the axions originate from the Sun there is necessarily some model dependence in extracting such bounds; the high plasma frequency and temperature in the Sun are particularly relevant as these can perturb the effective axion-photon coupling [19, 30]. Moreover bounds derived from stellar cooling arguments, e.g. neutrino observations of Supernova 1987a, have large astrophysical uncertainties [31].

By contrast in laboratory experiments the axion production process is directly controlled, avoiding such model dependence. Interesting constraints have been set by accelerator experiments, such as Belle II [32] and NA64 [33]. Laboratory-based searches for axions are thus well motivated even though they do not presently reach the same sensitivity as astrophysical limits.

Here we present results from a new laboratory search for axions performed with the HED/HiBEF instrument at the EuXFEL in Hamburg [34]. This is sensitive to a broad range of axion/ALP mass, in the range  $\sim 10^{-3}$  –  $10^4$  eV. Our experiment exploits the Primakoff effect via which photons can decay into axions in the presence of a strong external electric field and then reconvert back into photons after passing through an opaque wall. This technique has previously been employed in experiments with optical lasers and external magnetic fields [35–37].

When using X-rays, it is possible to increase the detection sensitivity by exploiting the electric fields which are present within a crystalline material. These atomic electric fields can be as high as  $10^{11}$  V m<sup>-1</sup>, which corresponds to magnetic field strengths of order 1 kT – much

higher than the field strengths accessible using the best electromagnets. Furthermore, arranging atoms in a crystalline structure leads to a coherent effect analogous to Bragg scattering. Generation and reconversion can thus be carried out with a pair of X-ray crystals. This concept was first described by Buchmüller & Hoogeveen [38].

We improve on previous laboratory-based searches in the above mass range (up to which were performed using 3<sup>rd</sup> generation synchrotron facilities [1, 39] but we achieve higher detection sensitivity due to the increased brightness of Free Electron Lasers (FELs). This is because of the much shorter duration of the photon pulse which allows for a more accurate discrimination of the signal against the background.

*Experimental setup.* As discussed, a number of experiments have already placed bounds on the available axion parameter space, with varying degrees of model dependence. We use the term axion to describe both the QCD axion and any ALP which couples to photons via the dimension-5 operator

$$\mathcal{L}_{\text{axion}} = g_{a\gamma\gamma} \mathbf{E} \cdot \mathbf{B} a, \quad (1)$$

where  $\mathbf{E}$  is the electric field in the crystal lattice,  $\mathbf{B}$  is the magnetic field associated with the electromagnetic wave of the X-ray photon,  $a$  is the  $CP$ -conserving scalar field of the axion, and  $g_{a\gamma\gamma}$  is the axion-photon coupling.

Experiments employing the above coupling exploit the Primakoff effect viz. that there is a finite probability for a photon to decay into an axion in the presence of another photon, typically given by a static, external field. The conversion (or regeneration) probability is maximized when the electric and magnetic fields of these two photons are aligned. This probability increases linearly with interaction length.

The experimental setup is depicted in Figure 1. It shows two germanium (Ge) crystals oriented in Laue geometry, with their lattice planes parallel to one-another. The  $\sigma$ -polarised XFEL beam impinges on the first crystal from the left. The angle between the wave-vector of the incoming X-ray beam and the lattice planes in the crystals is denoted  $\theta$ . An important detail is that the Laue geometry is preferable to the more conventional Bragg scattering geometry because of the Borrmann effect, through which the transmission of X-rays in the Laue case is increased [38–41].

Both axions and Laue diffracted photons are transmitted through the first crystal. These are denoted respectively by  $a$  and  $\gamma$  in the figure. The photons are absorbed by a radiation shield but the weakly interacting axions impinge on the second crystal. Here the strong electric field enables the regeneration of photons via the inverse Primakoff process. These regenerated photons are observed by a detector downstream of the crystals. In the configuration where  $\theta = \theta_B$  (here  $\theta_B$  is the Bragg angle), the design is sensitive to a broad range of axion mass  $m_a$  satisfying the inequality

$$|m_a^2 - m_\gamma^2| \lesssim \frac{4k_\gamma}{L_{\text{eff}}}, \quad (2)$$

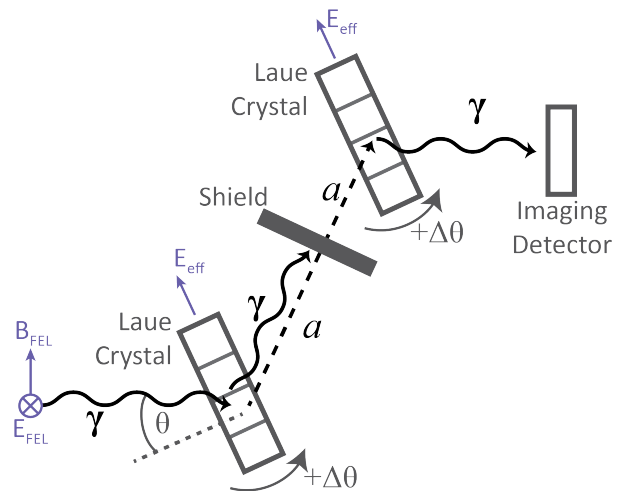


FIG. 1. Diagram of the setup in our experiment; the X-ray beam propagates from left to right. Axion production and photon regeneration are expected to take place via the effective electric field within a pair of monolithic crystals, Ge (220) in Laue geometry, with dimensions: 10 mm  $\times$  10 mm  $\times$  0.5 mm. A pair of piezoelectric rotation stages (Xeryon, XRT-U30) were used to orient the germanium crystals. The radiation shield is a 1 mm thick titanium sheet.

where  $m_\gamma = 44$  eV is the plasma frequency of the valence electrons in the conversion crystals [39];  $k_\gamma$  is the photon energy; and  $L_{\text{eff}}$  is the effective path length of X-rays within a crystal. We use units where  $\hbar = c = 1$ .

In the case where there is a detuning from the Bragg angle, by  $\Delta\theta = \theta - \theta_B$ , it can be shown [39, 41] that the setup becomes sensitive to a narrow range of axion mass ( $\Delta m_a \sim 10^{-3}$  eV) centered on

$$m_a = \sqrt{m_\gamma^2 + 2q_T k_\gamma \cos(\theta_B) \Delta\theta}, \quad (3)$$

where  $q_T = 6.20$  keV [39] is the magnitude of the reciprocal lattice vector. This means that by sweeping through different values of  $\Delta\theta$  it is possible to search for heavy axions with mass in the interval between the plasma frequency of the crystal and the projection of the incoming photon energy onto the reciprocal lattice vector.

The EuXFEL was operated in a seeded mode, with 9.8 keV photon energy (wavelength,  $\lambda_x = 2\pi/k_\gamma = 1.265$  Å). The repetition rate was 10 Hz, with one pulse per train. The X-ray beam was collimated by upstream compound refractive lenses (CRLs). The full-width-half-maximum of the beam transverse profile was measured to be 400  $\mu\text{m}$  at the center of the interaction chamber. The axion-photon conversion probability  $P(a \leftrightarrow \gamma)$  for Laue-case diffraction is given by [39]

$$P(a \leftrightarrow \gamma) = \left( \frac{1}{4} g_{a\gamma\gamma} E_{\text{eff}} L_{\text{eff}} \cos \theta_B \right)^2, \quad (4)$$

where  $E_{\text{eff}} = 7.3 \times 10^{10}$  V/m is the crystalline electric

field [39], and

$$L_{\text{eff}} = 2L_{\text{att}}^B \left(1 - e^{-L_x/2L_{\text{att}}^B}\right), \quad (5)$$

where  $L_x = t/\cos(\theta_B + \Delta\theta)$  is the X-ray path length inside the crystals ( $t = 500 \mu\text{m}$  is the thickness of each crystal) and  $L_{\text{att}}^B = 1499.8 \mu\text{m}$  (for  $\sigma$ -polarization) [42].

For a short X-ray pulse the rocking curve of the crystal has a width dictated by the characteristic timescale of the scattering process,  $\Delta\theta_{RC} = \lambda_x \tan \theta_B / \Delta T$  [43, 44]. Because of the Borrmann effect, the extinction length of the X-rays is longer than the X-ray path-length in the crystal and therefore the characteristic timescale is simply given by the geometric time-delay due to scattering off multiple planes,

$$\Delta T = 2t \tan \theta_B \sin \theta_B. \quad (6)$$

The resulting rocking curve ( $\Delta\theta_{RC} \sim 0.4 \mu\text{rad}$ ) is narrower than the Darwin width,  $\Delta\theta_D = 44 \mu\text{rad}$  for Ge (220), and the diffracted X-ray pulse becomes transform limited. As shown in Ref. [39], the effective conversion length,  $L_{\text{eff}}$ , is inversely proportional to the width of the rocking curve, and in deriving Eq. (4) it was assumed that this is just the Darwin width. This narrowing of the rocking curve implies that the interaction amplitude must increase by a factor  $\xi_B = \Delta\theta_D/\Delta\theta_{RC}$  as a consequence of the modified susceptibility for the Laue-case diffraction. Thus, the scattering probability becomes [45]

$$P(a \leftrightarrow \gamma) = \left(\frac{1}{4} g_{a\gamma\gamma} E_{\text{eff}} L_{\text{eff}} \xi_B \cos \theta_B\right)^2. \quad (7)$$

The regenerated photons were measured using a silicon hybrid-pixel JUNGFRU detector [46]. The JUNGFRU was operated in a time-gated mode with an acquisition time of  $2 \mu\text{s}$ , centered on the X-ray pulse trains. The device was absolutely calibrated to provide an energy resolution better than  $0.5 \text{ keV}$ . To mitigate the presence of scattered light, the detector was separated from the interaction region by a  $6 \text{ m}$  evacuated flight tube, and motorised slits ( $2 \text{ mm}$  tungsten) were used to baffle the input to this tube.

*Photon flux limits.* The sensitivity of the experiment was limited by X-ray heating in the axion generation crystal. This alignment instability is attributed to distortions to the crystal structure, induced by thermal expansion under the heat load of the X-ray flux. To reduce the effect of heating, the experiment was performed after attenuating the X-ray flux by a factor of  $10^3$ . Under these conditions, the alignment of the system was preserved for a period of  $\sim 10 \text{ min}$ , with the transmission through the setup fluctuating at the  $10\%$  level.

In order to ensure that alignment stability was maintained over a cumulative acquisition period of the order of hours, we adopted the technique depicted graphically in Figure 2. This data shows the normalised intensity measured on the downstream JUNGFRU during a run dedicated to axion detection, which was separated into three distinct phases:

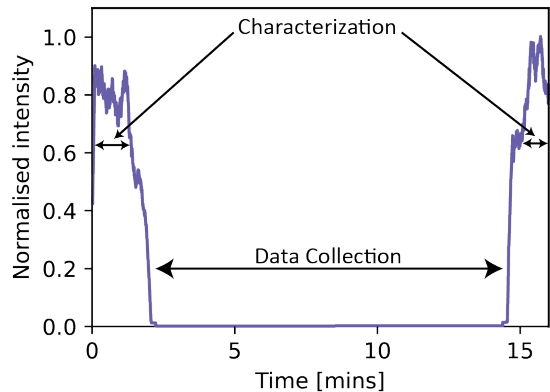


FIG. 2. A plot of the time resolved X-ray intensity measured by the JUNGFRU in a single data acquisition period. The data shows that the run was split into two periods devoted to instrument characterisation, separated by a single period in which the instrument was setup to search for axions.

$\Delta\theta$ [mrad]	$m_a$ [eV]	$N_{\text{in}} (\times 10^{16})$	$g_{a\gamma\gamma}$ [ $\text{GeV}^{-1}$ ]
0.0	$\lesssim 44$	2.6	$3.91 \times 10^{-4}$
1.0	$3.4 \times 10^2$	2.4	$3.10 \times 10^{-4}$
1.8	$4.6 \times 10^2$	1.6	$3.87 \times 10^{-4}$
10.0	$1.1 \times 10^3$	1.7	$3.69 \times 10^{-4}$
50.0	$2.4 \times 10^3$	1.5	$2.76 \times 10^{-4}$

TABLE I. Summary of the different runs which were performed during the experiment. The detuning angles,  $\Delta\theta$ ; corresponding masses,  $m_a$ ; total number of photons incident upon the apparatus,  $N_{\text{in}}$ ; and inferred bound on the strength of the axion-photon coupling constant,  $g_{a\gamma\gamma}$  are indicated.

1. The setup was tuned to the Bragg angle, and the radiation shield was removed from the optical path. The device was operated in this mode for  $\sim 2 \text{ min}$  and the data from this interval were used to characterise the transmission through the setup.
2. The rotation stages were detuned to the search angle, and the radiation shield was scrolled into the optical path. Data were collected in this configuration for  $\sim 10 \text{ min}$  – this represents the period in which the instrument was searching for axions.
3. The setup was tuned back to the Bragg angle and the radiation shield was scrolled out. Then another  $\sim 2 \text{ min}$  of characterisation data were acquired.

If heating had caused the Bragg angle of the first crystal to change significantly between the two characterisation phases, then the axion search data were disregarded and the rotation of the first crystal was adjusted to the new Bragg angle before the start of the next run.

*Results.* Our search was limited to 5 discrete  $\Delta\theta$  values, with data collected for  $60 - 90 \text{ min}$  at each angle. Table I, shows the bounds on the axion-photon coupling determined from our data at each detuning angle.

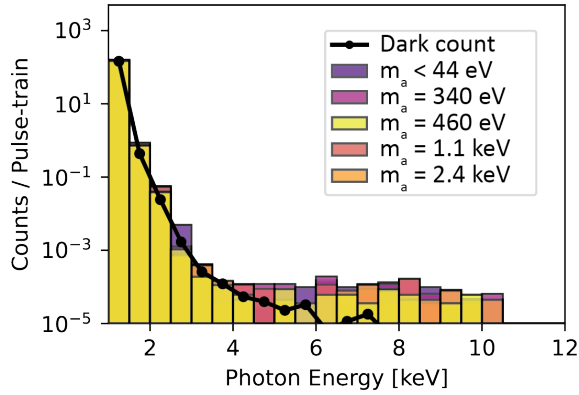


FIG. 3. A histogram showing the events detected across all acquisitions and over the whole detector area. The number of counts in a 24 hour dark run are also shown.

Figure 3 is a histogram which shows energy-resolved events for each of the data sets which are detailed in Table I. These are compared against the number of counts in a 24-hour long dark-run. ALP observations can be distinguished from the background as reconverted X-rays must be identical to the primary EuXFEL X-rays, and moreover must fall inside the region on the detector which is impacted by the X-ray beam when the shield is absent.

To establish if any of the few events in the relevant energy band do fall upon the X-ray spot, and therefore might be associated with axion production, hit-maps of spatially resolved events were produced. Figure 4 is an example of such analysis. In this figure the blue colour map shows transmission through the setup in the absence of the radiation shield. The data points overlaid on the colour map indicate the location of hits on the detector with a photon energy exceeding 4 keV for each of the data sets in Table I.

As Figure 4 shows, there are no events which overlap with the region of the X-ray spot (the darker blue region in the center of the figure). The absence of any such events implies that no events consistent with axion production were detected during the experiment. The limit which can be placed on the axion-photon coupling is then obtained by inverting Eq. (7):

$$g_{a\gamma\gamma} < \left( \frac{1}{4} E_{\text{eff}} L_B \xi_B \cos \theta_B \right)^{-1} P(a \leftrightarrow \gamma)^{1/2}, \quad (8)$$

with  $P(a \leftrightarrow \gamma)^2 = (N_{\text{det}}/\eta N_{\text{in}})$ ;  $N_{\text{det}}$  is the detected number of photons;  $N_{\text{in}}$  is the number of input photons.

The efficiency factor  $\eta$  accounts for losses associated with the deviation from parallelism between the two crystals; fluctuations in the exact X-ray energy; and the quantum efficiency of the detector. The value of  $\eta$  was obtained experimentally. As described above and shown in Figure 2, the data collection was split into 10 minute runs. At the beginning and end of each run, the crystals were tuned to the Bragg angle and the radiation

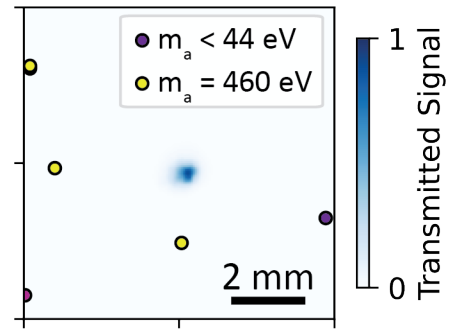


FIG. 4. An image showing the transmitted signal obtained in the absence of the radiation shield (blue colour-map) overlaid by the position of  $k_\gamma \geq 4$  keV events across all data acquisitions. A fiducial indicating scale on the detector plane is also shown.

shield was removed in order to characterise the experimental setup. During these characterisation phases, the efficiency factor for the  $i$ -th run at a given detuning angle,  $\eta_i$ , was given by

$$\eta_i = \frac{1}{T_{\text{Ge}}^2} \frac{E_i^{\text{JF, ch}}}{E_i^{\text{in, ch}}}, \quad (9)$$

where  $T_{\text{Ge}}$  is the transmission factor associated with a single crystal;  $E_i^{\text{JF, ch}}$  is the total X-ray dose measured on the (downstream) JUNGFRAU detector during these characterisation phases; and  $E_i^{\text{in, aq}}$  is the total X-ray dose measured (during characterisation) on a passive upstream monitor [47].

Because of the very narrow rocking curve for Laue-case diffraction, a single Ge crystal can be used to determine the EuXFEL spectral profile by detuning it from the Bragg angle and recording the transmitted intensity on a separate JUNGFRAU detector as a function of the detuning angle. This is shown in Figure 5, where the seeded X-ray beam is shown to have an energy bandwidth of  $\Delta E/E = \Delta \theta_s / \tan \theta_B = 5.2 \times 10^{-5}$ , or  $\sim 0.5$  eV at 9.8 keV. This is indeed expected for a self-seeded beam [48], and the variations in the transmitted intensity are associated with shot-to-shot variability in the exact seeded pulse energy. Overall, the transmission through a single crystal is determined to be of order  $T_{\text{Ge}} \approx 3 \times 10^{-3}$ .

For the data collection phases of a given dataset, the value of  $\eta N_{\text{in}}$  was then taken as

$$\eta N_{\text{in}} = \sum_i \eta_i E_i^{\text{in, aq}} / k_\gamma, \quad (10)$$

where the summation is across all runs at a given detuning angle;  $E_i^{\text{in, aq}}$  is the dose measured on the passive upstream monitor during data collection; and  $k_\gamma = 9.8$  keV is the photon energy. To derive a bound based on the observation of zero events consistent with axion production, we take the 90% confidence upper limit to be  $N_{\text{det}} = 2.3$  events.

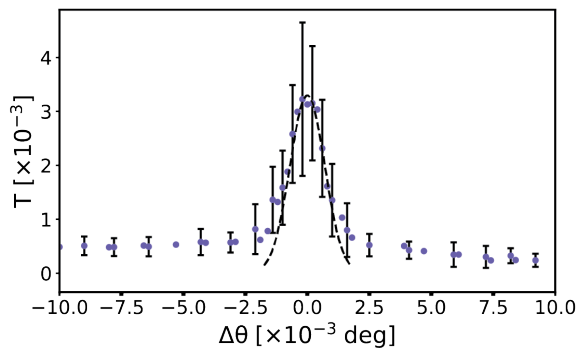


FIG. 5. X-ray transmission through a single Ge crystal as a function of the detuning angle  $\Delta\theta$ . The central peak is fitted with a Gaussian (dashed line) of width  $\Delta\theta_s \approx 17.4 \mu\text{rad}$ . An average of 145 shots per angular point are used to construct the peak curve, while 32 shots are used for each angular point on the baseline. The error bars on the measurements are  $1\sigma$ .

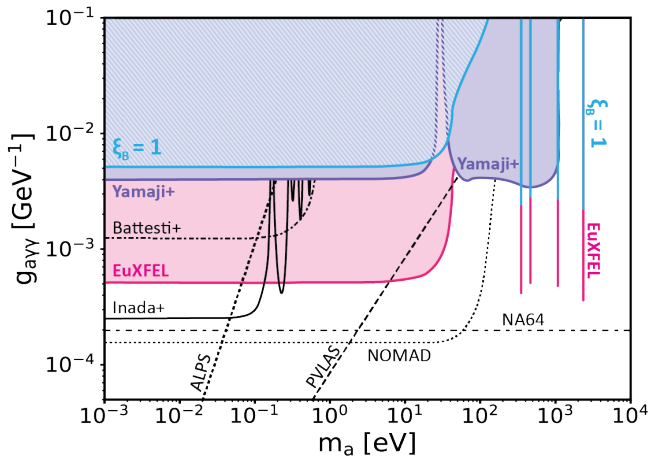


FIG. 6. Bounds on the axion-photon coupling from our experiment (pink), compared with those from Yamaji et al. [1, 39] (purple). The excluded reegion taking  $\xi_B = 1$  in Eq. (8) is also plotted (blue). Shown for comparison are bounds from other laboratory searches: NOMAD [49], PVLAS [50], ALPS [36], NA64 [33], Battesti et al. [51] and Inada et al. [52].

*Concluding remarks.* The outcome of this analysis of data collected at EuXFEL is shown in Figure 6, which summarizes bounds in the meV–few keV mass range, from searches for laboratory-generated axions. We were able to improve on the results from Ref. [1] at several discrete axion masses, and also to probe a previously unconstrained axion mass of  $m_a = 2.4 \text{ keV}$ . For  $m_a \gtrsim 200 \text{ eV}$ , we were able to surpass the sensitivity of bounds from all

previous searches for laboratory-generated axions, viz. NOMAD [49], PVLAS [50], ALPS [36], Battesti et al. [51], Inada et al. [52], except NA64 [33].

We emphasise that this is not the best sensitivity achievable with the present setup. As discussed above, issues with X-ray heating forced us to attenuate the X-ray flux by a factor of  $10^3$ . Moreover, the X-ray bunch structure was set with the number of pulses per train limited to 1, out of a possible 300. Issues with retaining alignment also limited data acquisition time to 60–90 min at each detuning angle; with a more stable setup that would include active cooling of the first conversion crystal, these times could be increased by a factor of 30. Furthermore, we could also fully exploit the Borrmann effect and use Ge crystals up to 1.5 mm in thickness. Taken together these improvements would increase the sensitivity by a factor  $\sim 150$ , bringing the estimated bounds down to  $2 \times 10^{-6} \text{ GeV}^{-1}$ , close to the expectation for QCD axions to be dark matter [53]. Below  $\sim 1 \text{ eV}$ , these bounds are also comparable to proposed photon regeneration experiments using superconducting pulsed magnetic fields [54]. Currently no other laboratory-based technique has such sensitivity in the  $\gtrsim 10 \text{ eV}$  mass range.

## ACKNOWLEDGEMENTS

This research received funding from the UK Engineering and Physical Sciences Research Council (grants EP/X01133X/1 & EP/X010791/1). SS and GG are members of the ‘Quantum Sensors for the Hidden Sector’ consortium funded by the UK Science & Technology Facilities Council (grant ST/T006277/1). JH was partially supported by the US Defence Threat Reduction Agency (award HDTRA1-20-1-0001) and the US Department of Energy (awards DE-SC0020434 & DE-NA0003764). CH was partly funded through the UK XFEL Physical Sciences Hub.

We acknowledge the European XFEL in Schenefeld, Germany for the provision of beamtime at HED SASE2 and thank the staff for their assistance.

GG and SS would like to thank Andreas Ringwald for helpful comments.

## DATA AVAILABILITY

The raw data recorded for this experiment at the European XFEL are available at DOI:10.22003/XFEL.EU-DATA-003326-00.

[1] T. Yamaji, K. Tamasaku, T. Namba, T. Yamazaki, and Y. Seino, Search for Axion like particles using Laue-case conversion in a single crystal, Phys. Lett. B **782**, 523 (2018), arXiv:1802.08388 [hep-ex].

[2] R. D. Peccei and H. R. Quinn, CP Conservation in the Presence of Instantons, Phys. Rev. Lett. **38**, 1440 (1977).

[3] S. Weinberg, A New Light Boson?, Phys. Rev. Lett. **40**, 223 (1978).

- [4] F. Wilczek, Problem of Strong  $P$  and  $T$  Invariance in the Presence of Instantons, *Phys. Rev. Lett.* **40**, 279 (1978).
- [5] P. Svrcek and E. Witten, Axions In String Theory, *JHEP* **06**, 051, arXiv:hep-th/0605206.
- [6] J. Preskill, M. B. Wise, and F. Wilczek, Cosmology of the Invisible Axion, *Phys. Lett. B* **120**, 127 (1983).
- [7] L. F. Abbott and P. Sikivie, A Cosmological Bound on the Invisible Axion, *Phys. Lett. B* **120**, 133 (1983).
- [8] M. Dine and W. Fischler, The Not So Harmless Axion, *Phys. Lett. B* **120**, 137 (1983).
- [9] P. Sikivie, Experimental Tests of the Invisible Axion, *Phys. Rev. Lett.* **51**, 1415 (1983), [Erratum: *Phys.Rev.Lett.* 52, 695 (1984)].
- [10] Y. K. Semertzidis and S. Youn, Axion dark matter: How to see it?, *Sci. Adv.* **8**, abm9928 (2022), arXiv:2104.14831 [hep-ph].
- [11] J. E. Kim, Weak Interaction Singlet and Strong CP Invariance, *Phys. Rev. Lett.* **43**, 103 (1979).
- [12] M. Dine, W. Fischler, and M. Srednicki, A Simple Solution to the Strong CP Problem with a Harmless Axion, *Phys. Lett. B* **104**, 199 (1981).
- [13] A. R. Zhitnitsky, On Possible Suppression of the Axion Hadron Interactions. (In Russian), *Sov. J. Nucl. Phys.* **31**, 260 (1980).
- [14] A. Ringwald and K. Saikawa, Axion dark matter in the post-inflationary Peccei-Quinn symmetry breaking scenario, *Phys. Rev. D* **93**, 085031 (2016), [Addendum: *Phys.Rev.D* 94, 049908 (2016)], arXiv:1512.06436 [hep-ph].
- [15] K. A. Beyer and S. Sarkar, Ruling out light axions: The writing is on the wall, *SciPost Phys.* **15**, 003 (2023), arXiv:2211.14635 [hep-ph].
- [16] M. Kamionkowski and J. March-Russell, Planck scale physics and the Peccei-Quinn mechanism, *Phys. Lett. B* **282**, 137 (1992), arXiv:hep-th/9202003.
- [17] R. Holman, S. D. H. Hsu, T. W. Kephart, E. W. Kolb, R. Watkins, and L. M. Widrow, Solutions to the strong CP problem in a world with gravity, *Phys. Lett. B* **282**, 132 (1992), arXiv:hep-ph/9203206.
- [18] S. M. Barr and D. Seckel, Planck scale corrections to axion models, *Phys. Rev. D* **46**, 539 (1992).
- [19] A. Caputo and G. Raffelt, Astrophysical Axion Bounds: The 2024 Edition, *PoS COSMICWISPErs*, 041 (2024), arXiv:2401.13728 [hep-ph].
- [20] V. Anastassopoulos *et al.* (CAST), New CAST Limit on the Axion-Photon Interaction, *Nature Phys.* **13**, 584 (2017), arXiv:1705.02290 [hep-ex].
- [21] F. T. Avignone, III *et al.* (SOLAX), Experimental search for solar axions via coherent Primakoff conversion in a germanium spectrometer, *Phys. Rev. Lett.* **81**, 5068 (1998), arXiv:astro-ph/9708008.
- [22] R. Bernabei *et al.*, Search for solar axions by Primakoff effect in NaI crystals, *Phys. Lett. B* **515**, 6 (2001).
- [23] A. Morales *et al.* (COSME), Particle dark matter and solar axion searches with a small germanium detector at the Canfranc Underground Laboratory, *Astropart. Phys.* **16**, 325 (2002), arXiv:hep-ex/0101037.
- [24] Z. Ahmed *et al.* (CDMS), Search for Axions with the CDMS Experiment, *Phys. Rev. Lett.* **103**, 141802 (2009), arXiv:0902.4693 [hep-ex].
- [25] P. Belli, R. Bernabei, F. Cappella, R. Cerulli, F. A. Danevich, A. Incicchitti, V. V. Kobychev, M. Laubenstein, O. G. Polischuk, and V. I. Tretyak, Search for Li-7 solar axions using resonant absorption in LiF crystal: Final results, *Phys. Lett. B* **711**, 41 (2012).
- [26] E. Armengaud *et al.*, Axion searches with the EDELWEISS-II experiment, *JCAP* **11**, 067, arXiv:1307.1488 [astro-ph.CO].
- [27] I. J. Arnquist *et al.* (Majorana), Search for Solar Axions via Axion-Photon Coupling with the Majorana Demonstrator, *Phys. Rev. Lett.* **129**, 081803 (2022), arXiv:2206.05789 [nucl-ex].
- [28] E. Aprile *et al.* (XENON), Search for New Physics in Electronic Recoil Data from XENONnT, *Phys. Rev. Lett.* **129**, 161805 (2022), arXiv:2207.11330 [hep-ex].
- [29] J. B. Dent, B. Dutta, and A. Thompson, Bragg-Primakoff Axion Photoconversion in Crystal Detectors, (2023), arXiv:2307.04861 [hep-ph].
- [30] J. Jaeckel, E. Masso, J. Redondo, A. Ringwald, and F. Takahashi, The Need for purely laboratory-based axion-like particle searches, *Phys. Rev. D* **75**, 013004 (2007), arXiv:hep-ph/0610203.
- [31] N. Bar, K. Blum, and G. D'Amico, Is there a supernova bound on axions?, *Phys. Rev. D* **101**, 123025 (2020), arXiv:1907.05020 [hep-ph].
- [32] M. J. Dolan, T. Ferber, C. Hearty, F. Kahlhoefer, and K. Schmidt-Hoberg, Revised constraints and Belle II sensitivity for visible and invisible axion-like particles, *JHEP* **12**, 094, [Erratum: *JHEP* 03, 190 (2021)], arXiv:1709.00009 [hep-ph].
- [33] D. Banerjee *et al.* (NA64), Search for Axionlike and Scalar Particles with the NA64 Experiment, *Phys. Rev. Lett.* **125**, 081801 (2020), arXiv:2005.02710 [hep-ex].
- [34] U. Zastrau, K. Appel, C. Baetz, O. Baehr, L. Batchelor, A. Berghäuser, M. Banjafar, E. Brambrink, V. Cerantola, T. E. Cowan, *et al.*, The High Energy Density Scientific Instrument at the European XFEL, *Journal of Synchrotron Radiation* **28**, 1393 (2021).
- [35] C. Robilliard, R. Battesti, M. Fouche, J. Mauchain, A.-M. Sautivet, F. Amiranoff, and C. Rizzo, No light shining through a wall, *Phys. Rev. Lett.* **99**, 190403 (2007), arXiv:0707.1296 [hep-ex].
- [36] K. Ehret *et al.*, New ALPS Results on Hidden-Sector Lightweights, *Phys. Lett. B* **689**, 149 (2010), arXiv:1004.1313 [hep-ex].
- [37] R. Ballou *et al.* (OSQAR), New exclusion limits on scalar and pseudoscalar axionlike particles from light shining through a wall, *Phys. Rev. D* **92**, 092002 (2015), arXiv:1506.08082 [hep-ex].
- [38] W. Buchmuller and F. Hoogeveen, Coherent Production of Light Scalar Particles in Bragg Scattering, *Phys. Lett. B* **237**, 278 (1990).
- [39] T. Yamaji, T. Yamazaki, K. Tamasaku, and T. Namba, Theoretical calculation of coherent Laue-case conversion between x-rays and ALPs for an x-ray light-shining-through-a-wall experiment, *Phys. Rev. D* **96**, 115001 (2017), arXiv:1709.03299 [physics.ins-det].
- [40] E. K. Kovev, O. N. Efimov, and L. I. Korovin, Characteristics of anomalous transmission of x-rays in the general case of laue diffraction, *Physica Status Solidi (b)* **35**, 455 (1969).
- [41] W. Liao, Generation and search of axion-like light particle using intense crystalline field, *Phys. Lett. B* **702**, 55 (2011), arXiv:1011.6460 [hep-ph].
- [42] From <https://x-server.gmca.aps.anl.gov/x0h.html>.
- [43] J. Wark and R. Lee, Simulations of femtosecond X-ray diffraction from unperturbed and rapidly heated single crystals, *Journal of Applied Crystallography* **32**, 692

- (1999).
- [44] Y. Shvyd'ko and R. Lindberg, Spatiotemporal Response of Crystals in X-ray Bragg Diffraction, *Phys. Rev. ST Accel. Beams* **15**, 100702 (2012), arXiv:1207.3376 [physics.optics].
- [45] A derivation of this would require full solution of the time-dependent dynamical diffraction equations, which is outside the scope of the present work.
- [46] A. Mozzanica, A. Bergamaschi, M. Brueckner, S. Cartier, R. Dinapoli, D. Greiffenberg, J. Jungmann-Smith, D. Maliakal, D. Mezza, M. Ramilli, C. Ruder, L. Schaedler, B. Schmitt, X. Shi, and G. Tinti, Characterization results of the jungfrau full scale readout asic, *Journal of Instrumentation* **11** (02), C02047.
- [47] T. Maltezopoulos, F. Dietrich, W. Freund, U. F. Jastrow, A. Koch, J. Laksman, J. Liu, M. Planas, A. A. Sorokin, K. Tiedtke, and J. Grünert, Operation of X-ray gas monitors at the European XFEL, *Journal of Synchrotron Radiation* **26**, 1045 (2019).
- [48] C. Emma, A. Lutman, M. W. Guetg, J. Krzywinski, A. Marinelli, J. Wu, and C. Pellegrini, Experimental demonstration of fresh bunch self-seeding in an X-ray free electron laser, *Appl. Phys. Lett.* **110**, 154101 (2017).
- [49] P. Astier *et al.* (NOMAD), Search for eV (pseudo)scalar penetrating particles in the SPS neutrino beam, *Phys. Lett. B* **479**, 371 (2000).
- [50] F. Della Valle, A. Ejlli, U. Gastaldi, G. Messineo, E. Milotti, R. Pengo, L. Piemontese, G. Ruoso, and G. Zavattini, New PVLAS model independent limit for the axion coupling to  $\gamma\gamma$  for axion masses above 1 meV, in *10th Patras Workshop on Axions, WIMPs and WISPs* (2014) pp. 67–70, arXiv:1410.4081 [hep-ex].
- [51] R. Battesti, M. Fouché, C. Detlefs, T. Roth, P. Berceau, F. Duc, P. Frings, G. L. J. A. Rikken, and C. Rizzo, Photon Regeneration Experiment for Axion Search Using X-Rays, *Physical Review Letters* **105**, 250405 (2010), 1008.2672.
- [52] T. Inada, T. Yamazaki, T. Namba, S. Asai, T. Kobayashi, K. Tamasaku, Y. Tanaka, Y. Inubushi, K. Sawada, M. Yabashi, T. Ishikawa, A. Matsuo, K. Kawaguchi, K. Kindo, and H. Nojiri, Search for Two-Photon Interaction with Axionlike Particles Using High-Repetition Pulsed Magnets and Synchrotron X Rays, *Physical Review Letters* **118**, 10.1103/physrevlett.118.071803 (2017).
- [53] C. A. J. O'Hare, Cosmology of axion dark matter, *PoS COSMICWISPs*, 040 (2024), arXiv:2403.17697 [hep-ph].
- [54] R. Rabadán, A. Ringwald, and K. Sigurdson, Photon Regeneration from Pseudoscalars at X-Ray Laser Facilities, *Physical Review Letters* **96**, 110407 (2005), hep-ph/0511103.